Siberian Branch of Russian Academy of Science
BUDKER INSTITUTE OF NUCLEAR PHYSICS

V. Telnov

PHOTON COLLIDER AT TESLA

BUDKER INP 2001-73

http://www.inp.nsk.su/publications

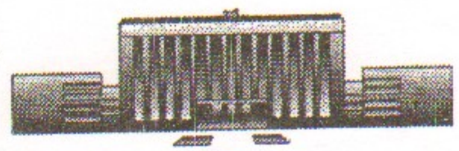

Novosibirsk
2001

Siberian Branch of Russian Academy of Science
BUDKER INSTITUTE OF NUCLEAR PHYSICS

V. Telnov

PHOTON COLLIDER AT TESLA

BUDKER INP 2001-73

http://www.inp.nsk.su/publications

Novosibirsk
2001

Photon collider at TESLA *

Valery Telnov
Institute of Nuclear Physics, 630090 Novosibirsk, Russia †

Abstract

Photon colliders ($\gamma\gamma$, γe) are based on backward Compton scattering of laser light off the high energy electrons in linear colliders. Recently the Technical Design Report of the linear collider TESLA has been published. In this paper physics program, possible parameters and some technical aspects the Photon Collider at TESLA are reviewed.

1 Introduction

Linear colliders, LC, at the center of mass energy from 100 GeV up to several TeV will be one of the central instruments in experimental high energy physics in the next 2 to 3 decades. Four projects are being developed: NLC [1], TESLA [2, 3], JLC [4], and CLIC [5]. In March 2001 the Technical Design of the linear collider TESLA on the energy 90–800 GeV has been published [3].

The unique feature of the e^+e^- Linear Colliders is the possibility to construct on its basis a Photon Collider using the process of the Compton backscattering of laser light off the high energy electrons [6, 7, 8]. Modern laser technology provides already the laser systems for collider photon colliders. This option is considered now for all linear colliders projects: NLC [1, 10, 9]; TESLA [11, 12, 13]; JLC [4, 14, 15]; CLIC [16]. The Photon Collider at TESLA discussed below has been included in the TESLA TDR though many aspects should be developed in more detail in the next 2–3 years.

The physics potential of the Photon Collider is very rich and complements in an essential way the physics program of the TESLA e^+e^- mode. A few examples:

- In $\gamma\gamma$ collisions, resonances with $\mathcal{C} = +$ are produced as single resonances. One of the most important examples is the Higgs boson. The precise knowledge of its two–photon width is of particular importance.

*Talk at the Snowmass Study on the Future of Particle Physics, Snowmass, USA, June 29-July 20, 2001

†email:telnov@inp.nsk.su

It is sensitive to heavy virtual charged particles. Supersymmetry predicts three neutral Higgs bosons. Photon colliders can produce the heavy neutral Higgs bosons with masses about 1.5 times higher than in e^+e^- collisions at the same collider.

- A $\gamma\gamma$ collider can produce pairs of any charged particles (charged Higgs, supersymmetric particles etc.) with a cross section about one order of magnitude higher than those in e^+e^- collisions. Moreover, the cross sections depend in a different form on various physical parameters. The polarization of the photon beams and the large cross sections allow to obtain valuable information on these particles and their interactions.
- At a γe collider charged particles can be produced with masses higher than in pair production of e^+e^- collisions (like a new W' boson and a neutrino or a supersymmetric scalar electron plus a neutralino).
- Photon colliders offer unique possibilities for measuring the $\gamma\gamma$ fusion of hadrons for probing the hadronic structure of the photon.

In the following we describe the physics programme, requirements for the lasers and possible laser and optical schemes, the expected $\gamma\gamma$ and γe luminosities at TESLA.

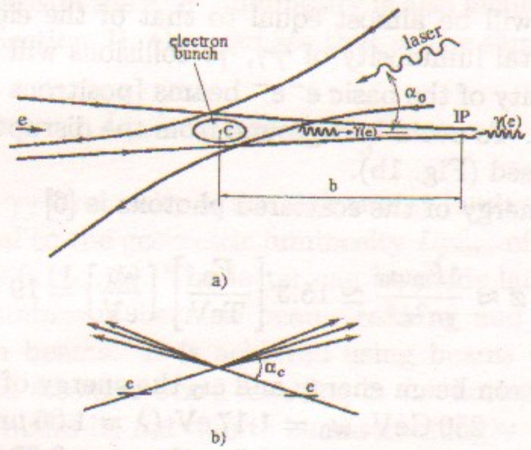

Figure 1: Scheme of $\gamma\gamma$, γe collider

The basic scheme of the Photon Collider is shown in Fig. 1. Two electron beams of energy E_0 after the final focus system travel towards the interaction point (IP) and at a distance b of about 1–5 mm from the IP collide with the focused laser beam. After scattering, the photons have an energy close to that of the initial electrons and follow their direction to the interaction point (IP) (with small additional angular spread of the order of $1/\gamma$, where

Table 1: Parameters of the Photon Collider based on TESLA.

$2E_0$, GeV	200	500	800
$L_{geom}, 10^{34}\,\mathrm{cm}^{-2}\mathrm{s}^{-1}$	4.8	12.0	19.1
$W_{\gamma\gamma,max}$, GeV	122	390	670
$L_{\gamma\gamma}(z > 0.8z_{m,\gamma\gamma}), 10^{34}\,\mathrm{cm}^{-2}\mathrm{s}^{-1}$	0.43	1.1	1.7
$W_{\gamma e,max}$, GeV	156	440	732
$L_{e\gamma}(z > 0.8z_{m,\gamma e}), 10^{34}\,\mathrm{cm}^{-2}\mathrm{s}^{-1}$	0.36	0.94	1.3
$L_{e^+e^-}, 10^{34}\,\mathrm{cm}^{-2}\mathrm{s}^{-1}$	1.3	3.4	5.8

$\gamma = E_0/mc^2$), where they collide with a similar opposite beam of high energy photons or electrons. Using a laser with a flash energy of several Joules one can "convert" almost all electrons to high energy photons. The photon spot size at the IP will be almost equal to that of the electrons at the IP and therefore the total luminosity of $\gamma\gamma$, γe collisions will be similar to the "geometric" luminosity of the basic e^-e^- beams (positrons are not necessary for photon colliders). To avoid background from the disrupted beams, a crab crossing scheme is used (Fig. 1b).

The maximum energy of the scattered photons is [6]

$$\omega_m = \frac{x}{x+1}E_0; \quad x \approx \frac{4E_0\omega_0}{m^2c^4} \simeq 15.3\left[\frac{E_0}{\mathrm{TeV}}\right]\left[\frac{\omega_0}{\mathrm{eV}}\right] = 19\left[\frac{E_0}{\mathrm{TeV}}\right]\left[\frac{\mu\mathrm{m}}{\lambda}\right], \tag{1}$$

where E_0 is the electron beam energy and ω_0 the energy of the laser photon. For example, for $E_0 = 250\,\mathrm{GeV}$, $\omega_0 = 1.17\,\mathrm{eV}$ ($\lambda = 1.06\,\mu\mathrm{m}$) (Nd:Glass and other powerful lasers) we obtain $x = 4.5$ and $\omega_m = 0.82E_0 = 205\,\mathrm{GeV}$ (it will be somewhat lower due to nonlinear effects in Compton scattering.

For increasing values of x the high energy photon spectrum becomes more peaked towards maximum energies. The value $x \approx 4.8$ is a good choice for photon colliders, because for $x > 4.8$ the produced high energy photons create QED e^+e^- pairs in collision with the laser photons, and as result the $\gamma\gamma$ luminosity is reduced [6, 8]. Hence, the maximum center of mass system energy in $\gamma\gamma$ collisions is about 80%, and in γe collisions 90% of that in e^+e^- collisions. If for some study lower photon energies are needed, one can

use the same laser and decrease the electron beam energy. The same laser with $\lambda \approx 1\,\mu\mathrm{m}$ can be used for all TESLA energies. At $2E_0 = 800\,\mathrm{GeV}$ the parameter $x \approx 7$, which is larger than 4.8. But nonlinear effects at the conversion region effectively increase the threshold for e^+e^- production, so that e^+e^- production is significantly reduced.

The luminosity distribution in $\gamma\gamma$ collisions has a high energy peak and a low energy part. The peak has a width at half maximum of about 15%. The photons in the peak can have a high degree of circular polarization. This peak region is the most useful for experimentation. When comparing event rates in $\gamma\gamma$ and e^+e^- collisions we will use the value of the $\gamma\gamma$ luminosity in this peak region $z > 0.8z_m$ where $z = W_{\gamma\gamma}/2E_0$.

The energy spectrum of high energy photons becomes most peaked if the initial electrons are longitudinally polarized and the laser photons are circularly polarized. This gives almost a factor of 3–4 increase of the luminosity in the high energy peak. The average degree of the circular polarization of the photons within the high-energy peak amounts to 90–95%. The sign of the polarization can easily be changed by changing the signs of electron and laser polarizations.

The luminosity expected at the TESLA Photon Collider are presented in Table 1, for comparison the e^+e^- luminosity is also included (a more detailed table is given in Section 3). One can see that at the same beam parameters

$$L_{\gamma\gamma}(z > 0.8z_m) \approx \frac{1}{3}L_{e^+e^-}. \tag{2}$$

Moreover, the $\gamma\gamma$ luminosity in the high energy luminosity peak for TESLA is just proportional to the geometric luminosity L_{geom} of the electron beams: $L_{\gamma\gamma}(z > 0.8z_m) \approx 0.1L_{geom}$. The latter can be made larger for $\gamma\gamma$ collisions than the e^+e^- luminosity because beamstrahlung and beam repulsion are absent for photon beams. It is achieved using beams with smallest possible emittances and stronger beam focusing in the horizontal plane (in e^+e^- collisions beams should be flat due to beamstrahlung).

Several examples of characteristic processes in $\gamma\gamma$, γe collisions at high energies are given below.

In the collision of photons any charged particle can be produced due to direct coupling. Neutral particles are produced via loops built up by charged particles ($\gamma\gamma \to$ Higgs, $\gamma\gamma, ZZ$). The cross sections for pairs of scalars, fermions or vector particles are all significantly larger (about one order of magnitude) in $\gamma\gamma$ collisions compared with e^+e^- collisions, as shown in Fig. 2 [8, 17]. For example, the maximum cross section for H^+H^- production with unpolarized photons is about 7 times higher than that in e^+e^-

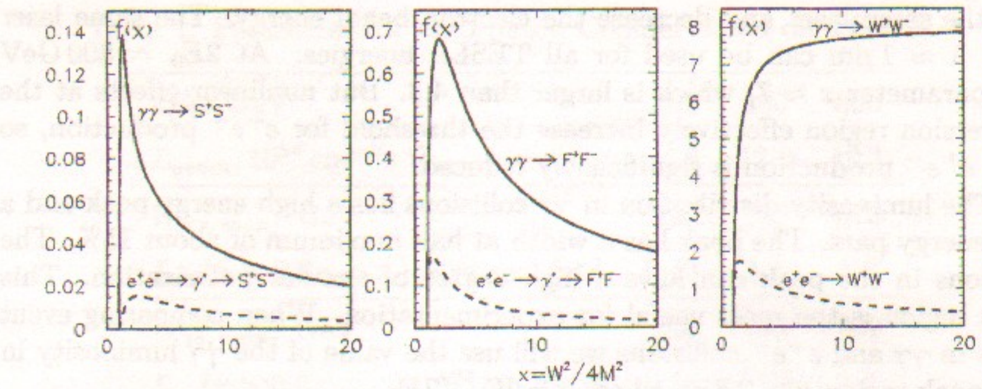

Figure 2: Comparison between cross sections for charged pair production in unpolarized e^+e^- and $\gamma\gamma$ collisions. S (scalars), F (fermions), W (W bosons); $\sigma = (\pi\alpha^2/M^2)f(x)$, M is the particle mass, W is the invariant mass.

collisions. With polarized photons and not far from threshold it is even larger by a factor of 20, Fig. 3 [18]. Using the luminosity given in the Table 1 the event rate is 8 times higher.

The two–photon production of pairs of charged particles is a pure QED process, while the cross section for pair production in e^+e^- collision is mediated by γ and Z exchange so that it depends also on the weak isospin of the produced particles. The e^+e^- process may also be affected by the exchange of new particles in the t–channel. Therefore, measurements of pair production both in e^+e^- and $\gamma\gamma$ collisions help to disentangle different couplings of the charged particles.

Another example is the direct resonant production of the Higgs boson in $\gamma\gamma$ collisions. It is evident from Fig. 4 [19], that the cross section at the photon collider is several times larger than the Higgs production cross section in e^+e^- collisions. Although the $\gamma\gamma$ luminosity is smaller than the e^+e^- luminosity (Table 1), the production rate of the Standard Model (SM) Higgs boson with mass between 120 and 250 GeV in $\gamma\gamma$ collisions is nevertheless about 1–10 times the rate in e^+e^- collisions at $2E_0 = 500$ GeV.

Photon colliders used in the γe mode can produce particles which are kinematically not accessible at the same collider in the e^+e^- mode. For example, in γe collisions one can produce a heavy charged particle in association with a light neutral one, such as supersymmetric selectron plus neutralino, $\gamma e \to \tilde{e}\tilde{\chi}^0$ or a new W' boson and neutrino, $\gamma e \to W'\nu$. In this way the discovery limits can be extended.

Based on these arguments alone, and without knowing *a priori* the particular scenario of new physics, there is a strong complementarity for e^+e^-

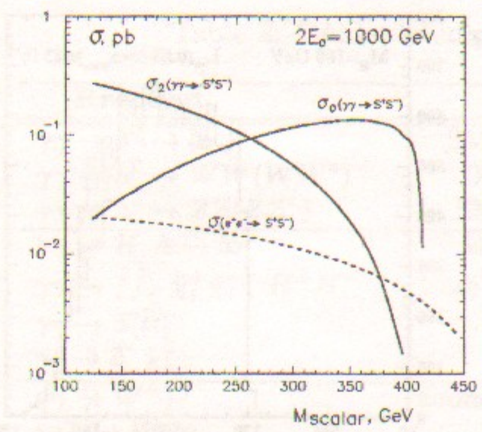

Figure 3: Pair production cross sections for charged scalars in e^+e^- and $\gamma\gamma$ collisions at $2E_0 = 1$ TeV collider (in $\gamma\gamma$ collision $W_{max} \approx 0.82$ TeV ($x = 4.6$)); σ_0 and σ_2 correspond to the total $\gamma\gamma$ helicity 0 and 2 respectively.

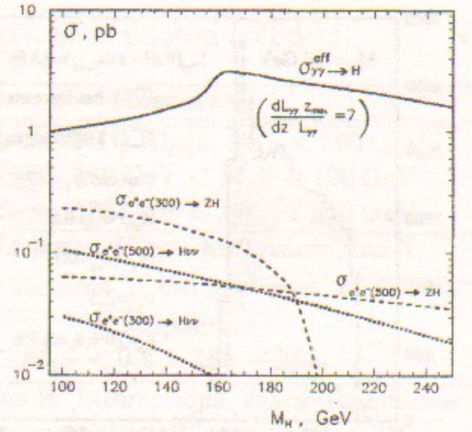

Figure 4: Total cross sections of the Higgs boson production in $\gamma\gamma$ and e^+e^- collisions. To obtain the Higgs boson production rate the cross section should be multiplied by the luminosity in the high energy peak $L_{\gamma\gamma}(z > 0.8z_m)$ given in the Table 1.

and $\gamma\gamma$ or γe modes for new physics searches.

2 The Physics

The two goals of studies at the next generation of colliders are the proper understanding of electroweak symmetry breaking, associated with the problem of mass, and the discovery of new physics beyond the Standard Model (SM). In both cases photon colliders can give considerable contributions.

The Higgs boson plays an essential role in the EWSB mechanism and the origin of mass. Precision electroweak data suggests that the Higgs boson is lighter than 200 GeV. The $\gamma\gamma$ collider option of a LC offers the unique possibility to produce the Higgs boson as an s–channel resonance [20]: $\gamma\gamma \to h^0 \to b\bar{b}, WW^*, ZZ, \tau\tau, gg, \gamma\gamma \ldots$. The Higgs production rate is proportional to $dL_{\gamma\gamma}/dW_{\gamma\gamma}$:

$$\dot{N}_{\gamma\gamma\to h} = L_{\gamma\gamma} \times \frac{dL_{\gamma\gamma}M_h}{dW_{\gamma\gamma}L_{\gamma\gamma}} \frac{4\pi^2\Gamma_{\gamma\gamma}(1+\lambda_1\lambda_2)}{M_h^3} \equiv L_{\gamma\gamma} \times \sigma^{eff}. \qquad (3)$$

$\Gamma_{\gamma\gamma}$ is the the two–photon width of the Higgs boson and λ_i are the photon helicities. The search and study of the Higgs boson can be carried out best by

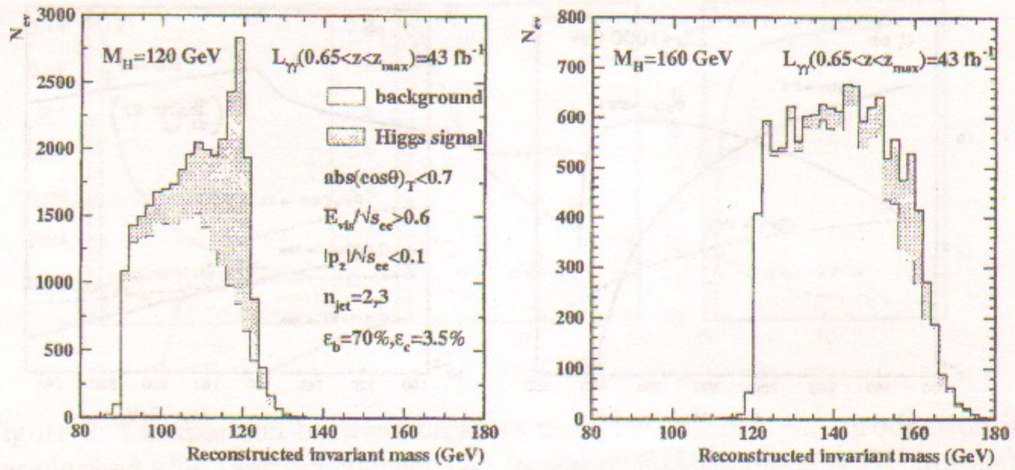

Figure 5: Mass distributions for the Higgs signal and heavy quark background for a) $M_h = 120\,GeV$ and b) $160\,GeV$.

exploiting the high energy peak of the $\gamma\gamma$ luminosity energy spectrum where $dL_{\gamma\gamma}/dW_{\gamma\gamma}$ has a maximum and the photons have a high degree of circular polarization. The effective cross section for $(dL_{\gamma\gamma}/dW_{\gamma\gamma})(M_h/L_{\gamma\gamma}) = 7$ and $1 + \lambda_1\lambda_2 = 2$ is presented in Fig. 4. As the luminosity is assumed the luminosity in the high energy luminosity peak ($z > 0.8z_m$).

The Higgs $\gamma\gamma$ partial width $\Gamma(h \to \gamma\gamma)$ is of special interest, since it is generated at the one–loop level including all heavy charged particles with masses generated by the Higgs mechanism and the cross section in $\gamma\gamma$ collisions is sensitive to contributions of new particles with masses beyond the energy covered directly by accelerators. Combined measurements of $\Gamma(h \to \gamma\gamma)$ at the photon collidrer and the branching ratio $\mathrm{BR}(h \to \gamma\gamma)$ at the e^+e^- and $\gamma\gamma$ LC provide a model–independent measurement of the total Higgs width.

$\mathcal{CP}$–parity of the Higgs boson can be measured using linearly polarized photon beams [21]. The cross section is proportional to $\sigma \propto 1 \pm l_{\gamma 1} l_{\gamma 2} \cos 2\phi$, where $l_{\gamma i}$ are degree of linear polarization and ϕ is the angle between $\vec{l_{\gamma 1}}$ and $\vec{l_{\gamma 2}}$; the $\pm$ signs correspond to $\mathcal{CP} = \pm 1$ scalar particles.

A light Higgs boson h with mass below the WW threshold can be detected in the $b\bar{b}$ decay mode. A Monte Carlo simulation of $\gamma\gamma \to h \to b\bar{b}$ for $M_h = 120$ and $160\,\mathrm{GeV}$ has been performed for an integrated luminosity in the high energy peak of $L_{\gamma\gamma}(0.8z_m < z < z_m) = 43\,\mathrm{fb}^{-1}$ in [22]. The results for the invariant mass distributions for the combined $b\bar{b}(\gamma)$ and $c\bar{c}(\gamma)$ backgrounds, after cuts, and for the Higgs signal are shown in Fig. 5.

This measurement together with the measurement of the $h \to b\bar{b}$ branching ratio in e^+e^- collisions will give the value of $\Gamma(h \to \gamma\gamma)$ with an accuracy

Table 2: Gold–plated processes at photon colliders

Reaction	Remarks
$\gamma\gamma \to h^0 \to b\bar{b}$	SM (or MSSM) Higgs, $M_{h^0} < 160\,\mathrm{GeV}$
$\gamma\gamma \to h^0 \to WW(WW^*)$	SM Higgs, $140\,\mathrm{GeV} < M_{h^0} < 190\,\mathrm{GeV}$
$\gamma\gamma \to h^0 \to ZZ(ZZ^*)$	SM Higgs, $180\,\mathrm{GeV} < M_{h^0} < 350\,\mathrm{GeV}$
$\gamma\gamma \to H, A \to b\bar{b}$	MSSM heavy Higgs, for interm. $\tan\beta$
$\gamma\gamma \to \tilde{f}\bar{\tilde{f}}$, $\tilde{\chi}_i^+\tilde{\chi}_i^-$, H^+H^-	large cr. sections, possible observ. of FCNC
$\gamma\gamma \to S[\tilde{t}\bar{\tilde{t}}]$	$\tilde{t}\bar{\tilde{t}}$ stoponium
$\gamma e \to \tilde{e}^-\tilde{\chi}_1^0$	$M_{\tilde{e}^-} < 0.9 \times 2E_0 - M_{\tilde{\chi}_1^0}$
$\gamma\gamma \to W^+W^-$	anomalous W interactions, extra dimensions
$\gamma e^- \to W^-\nu_e$	anomalous W couplings
$\gamma\gamma \to WWWW, WWZZ$	strong WW scatt., quar.anom. W, Z couplings
$\gamma\gamma \to t\bar{t}$	anomalous top quark interactions
$\gamma e^- \to \bar{t}b\nu_e$	anomalous Wtb coupling
$\gamma\gamma \to$ hadrons	total $\gamma\gamma$ cross section
$\gamma e^- \to e^- X$ and $\nu_e X$	$\mathcal{NC}$ and $\mathcal{CC}$ structure functions
$\gamma g \to q\bar{q}$, $c\bar{c}$	gluon distribution in the photon
$\gamma\gamma \to J/\psi\, J/\psi$	QCD Pomeron

of about 1% for the Higgs mass range between 120 and 140 GeV.

The SM Higgs boson with mass $135 < M_H < 190\,\mathrm{GeV}$ is expected to decay predominantly into WW^* or WW pairs. This decay mode should permit the detection of the Higgs boson signal below and slightly above the threshold of WW pair production [23]. It was shown that for $M_h = 160\,\mathrm{GeV}$ the product $\Gamma(h \to \gamma\gamma)\mathrm{BR}(h \to WW^*)$ can be measured at the Photon Collider with the statistical accuracy better than 2% at the integrated $\gamma\gamma$ luminosity of $40\,\mathrm{fb}^{-1}$ in the high energy peak. The branching ratio $\mathrm{BR}(WW^*)$ can be obtained from Higgs–strahlung in e^+e^- collisions with accuracy about 2%. Above the ZZ threshold and up to about 350–400 GeV the most promising channel to detect the Higgs signal is the reaction $\gamma\gamma \to ZZ$ [24].

Assuming that in addition to the measurement of the $h \to b\bar{b}$ branching ratio also the $h \to \gamma\gamma$ branching ratio can be measured (with an accuracy of 10–15%) at TESLA the total width of the Higgs boson can be determined in a model–independent way to an accuracy as dominated by the error on $\mathrm{BR}(h \to \gamma\gamma)$, the measurement of this branching ratio at the Photon Collider (normalised to $\mathrm{BR}(h \to b\bar{b})$ from the e^+e^- mode) will improve the accuracy of the total Higgs width.

Achievable accuracy of the two-photon Higgs width measurement is sufficient for distinquishing SM and 2HDM models [26].

In supersymmetric models at least five Higgs bosons are predicted: h^0, H^0, A^0, H^+, H^-. The Photon Collider has unique opportunities to search for the heavy neutral Higgs bosons in areas of SUSY parameter space not accessible elsewhere. Extensive studies have demonstrated that, while the light Higgs boson h of MSSM can be found at the LHC, the heavy bosons H and A may escape discovery for intermediate values of $\tan\beta$. At an e^+e^- LC the heavy MSSM Higgs bosons can only be found in associated production $e^+e^- \to HA$, with H and A having very similar masses. In the first phase of the LC with a total e^+e^-energy of 500 GeV the heavy Higgs bosons can thus be discovered for masses up to about 250 GeV. The mass reach can be extended by a factor of 1.6 in the $\gamma\gamma$ mode of TESLA, in which the Higgs bosons H, A can be singly produced.

The cross sections of the H, A signal in the $b\bar{b}$ decay mode and the corresponding background for the value of $\tan\beta = 7$ can be found elsewhere [25, 13]. The significance of the heavy Higgs boson signals is sufficient for a discovery of the Higgs particles with masses up to about 70–80% of the LC c.m.s. energy.

In $\gamma\gamma$ collisions, any kind of charged particle (supersymmetric, for example) can be produced in pairs, provided the mass is below the kinematical bound. For the $\gamma\gamma$ luminosity given in the Table 1, the production rates for these particles will be larger than that in e^+e^- collisions and detailed studies of the charged supersymmetric particles should be possible [28]. In addition, the cross sections in $\gamma\gamma$ collisions are given just by QED to leading order, while in e^+e^- collisions also Z boson and (sometimes) t–channel exchanges contribute. So, studying these processes in both channels provides complementary information about the interactions of the supersymmetric particles.

The γe collider could be the ideal machine for the discovery of scalar electrons ($\tilde{e}$) and neutrinos ($\tilde{\nu}$) in the reactions $\gamma e \to \tilde{e}^-\tilde{\chi}_1^0$, $\tilde{W}\tilde{\nu}$ [29]. Selectrons and neutralinos may be discovered in γe collisions up to the kinematical limit of $M_{\tilde{e}^-} < 0.9 \times 2E_0 - M_{\tilde{\chi}_i^0}$ where $2E_0$ is the energy of the original e^+e^- collider. This bound is larger than the bound obtained from $\tilde{e}^+\tilde{e}^-$ pair production in the e^+e^- mode, if $M_{\tilde{\chi}_i^0} < 0.4 \times 2E_0$.

In some scenarios of supersymmetric extensions of the Standard Model the stoponium bound states $\tilde{t}\bar{\tilde{t}}$ is formed. A photon collider would be the ideal machine for the discovery and study of these new narrow strong resonances [30].

New ideas have recently been proposed to explain the weakness of the gravitational force [31]. The Minkowski world is extended by extra space dimensions which are curled up at small dimensions R. Of the many processes examined so far, $\gamma\gamma \to WW$ provides the largest reach for extra dimension

energy scale for a given centre of mass energy of the LC [32]. The reach is in the range of $(11\text{–}13) \cdot 2E_0$. By comparison, a combined analysis of the processes $e^+e^- \to f\bar{f}$ with the same integrated luminosity leads to a reach of only $(6\text{–}7) \cdot 2E_0$.

Discussion of Gauge boson, top quark, QCD, hadron physics and other examples can be found elsewhere [33, 13, 34, 35]. A short list of processes which we think are the most important ones for the physics program of the Photon Collider option of the LC is presented in Table 2 [33]. Of course there exist many other possible manifestations of new physics in $\gamma\gamma$ and γe collisions which we have not discussed here.

3 The Interaction Region

3.1 The collision scheme, crab–crossing

The basic scheme for photon colliders is shown in Fig. 1. The distance between the conversion point (CP) and the IP, b, is chosen from the relation $b \approx \gamma\sigma_y$, so that the size of the photon beam at the IP has equal contributions from the electron beam size and the angular spread from Compton scattering. At TESLA $\sigma_y \approx 4\,\text{nm}$ gives $b \approx 2\,\text{mm}$ at $2E_0 = 500\,\text{GeV}$. Larger b values lead to a decrease of the $\gamma\gamma$ luminosity, for smaller b values the low–energy photons give a larger contribution to the luminosity (which is not useful for the experiment but causes additional backgrounds).

There are two additional constraints on the CP–IP distance. It should be larger than the half-length of the conversion region (which is about $Z_R \approx 0.35\,\text{mm}$ (Section 4)), and larger than about 2–3 σ_z (σ_z is the electron bunch length) because the $e \to \gamma$ conversion should take place before the beginning of electron beam repulsion. So, the minimum distance b for the TESLA is about 1 mm.

The removal of the disrupted beams can best be done using the crab-crossing scheme Fig. 1, which is foreseen in the NLC and JLC projects for e^+e^- collisions. Due to the collision angle the outgoing disrupted beams travel outside the final quads. The value of the crab–crossing angle is determined by the disruption angles and the final quad design (diameter of the quad and its distance from the IP). Simulation shows that the maximum disruption angle is about 10–11 mrad. Above this angle the total energy of particles is smaller than from unremovable e^+e^- pairs backgrounds. In the present TESLA design $\alpha_c = 34\,\text{mrad}$.

3.2 Collision effects, ultimate luminosities

At first sight, one may think that there are no collision effects in $\gamma\gamma$ and γe collisions because at least one of the beams is neutral. This is not correct because during the beam collision electrons and photons are influenced by the field of the opposite electron beam, which leads to the following effects [8]:

$\gamma\gamma$ collisions: conversion of photons into e^+e^- pairs (coherent pair creation).

γe collisions: coherent pair creation; beamstrahlung; beam displacement.

All these phenomena are understood analitically and have been included in simulation code. Beam collision effects in e^+e^- and $\gamma\gamma$, γe collisions are different. In particular, in $\gamma\gamma$ collisions there are no beamstrahlung or beam instabilities. Therefore, it was of interest to study limitations of the luminosity at the TESLA photon collider due to beam collision effects. The simulation was done for the TESLA beams and the horizontal size of the electron beams was varied. The results are the following (see graphs in [18, 12, 13]): all curves for the $\gamma\gamma$ luminosity follow their natural behaviour (as without collision effects): $L \propto 1/\sigma_x$ at least down to $\sigma_x = 10\,\mathrm{nm}$ (smaller values were not considered because too small horizontal sizes may introduce problems with the crab–crossing scheme). The $\gamma\gamma$ luminosity (in the high energy part) can reach the value 10^{35} $\mathrm{cm}^{-2}\mathrm{s}^{-1}$. Note that while in e^+e^- collisions $\sigma_x \approx 500\,\mathrm{nm}$, in $\gamma\gamma$ collisions the attainable σ_x with the planned injector (damping ring) is about 100 nm. In γe collisions the luminosity at small σ_x is lower than follows from the geometric scaling due to beamstrahlung and displacement of the electron beam during the beam collision. Its maximum value (high energy part) is about $(2\text{–}3)\cdot 10^{34}$ $\mathrm{cm}^{-2}\mathrm{s}^{-1}$.

So, we can conclude that for $\gamma\gamma$ collisions at TESLA one can use beams with a horizontal beam size down to 10 nm which is much smaller than that in e^+e^- collisions. Note, that the vertical beam size could also be additionally decreased by a factor of two (for even smaller electron beam size the effective photon beam size will be determined by the Compton scattering contribution). As a result, the $\gamma\gamma$ luminosity in the high energy peak can be, in principle, several times higher than the e^+e^- luminosity.

3.3 $\gamma\gamma$ and γe luminosities at TESLA

Parameters of the electron beams

Attainable $\gamma\gamma$ luminosity depends strongly on the emittances of the electron beams. There are two methods of production low–emittance electron beams: damping rings and low–emittance RF–photo–guns (without damping rings).

The second option is promising, but at the moment there are no such photo–guns producing polarized electron beams. Polarization of electron beams is very desirable for photon colliders. So, there is only one choice now — damping rings.

Especially for a photon collider the possibility of decreasing the beam emittances at the TESLA damping ring has been studied [39] and it was found that the horizontal emittance can be reduced by a factor of 4 compared to the previous design. Now the normalised horizontal emittance is $\epsilon_{nx} = 2.5 \times 10^{-6}\,\mathrm{m}$.

The luminosity also depends on the β–functions at the interaction points: $L \propto 1/\sqrt{\beta_x \beta_y}$. The vertical β_y is usually chosen close to the bunch length σ_z (this is the design for e^+e^- collisions and can also be realized for $\gamma\gamma$ collisions). Some questions remain about the minimum horizontal β–function. For e^+e^- collisions, $\beta_x \approx 15\,\mathrm{mm}$ which is larger than the bunch length $\sigma_z = 0.3\,\mathrm{mm}$, because beams in e^+e^- collisions must be flat to reduce beamstrahlung. In $\gamma\gamma$ collisions, β_x could be about 1 mm (or even somewhat smaller). There are two fundamental limitations: the beam length and the Oide effects (radiation in final quads). The latter is not important for the beam parameters considered. There is also a certain problem with the angular spread of the synchrotron radiation emitted in the final quads. But, for the photon collider the crab–crossing scheme will be used and in this case there is sufficient clearance for the removal of the disrupted beams and synchrotron radiation. Very preliminary studies of the existing scheme for the TESLA final focus have shown [40] that chromo–geometric aberrations dominate at $\beta \leq 6\,\mathrm{mm}$. Fortunately, a new scheme for the final focus system proposed at SLAC [41] (see also graphs in [13]) allows to obtain $\beta_x \approx 1.5\,\mathrm{mm}$ with small aberrations and further optimisation is possible. For the TDR study we assumed $\beta_x = 1.5\,\mathrm{mm}$.

$\gamma\gamma$, γe luminosities, summary table

The parameters of the photon collider at TESLA for $2E_0 = 200$, 500 and 800 GeV are presented in Table 3. For comparison the e^+e^- luminosity at TESLA is also included. It is assumed that the electron beams have 85% longitudinal polarization and that the laser photons have 100% circular polarization. The thickness of the laser target is one Compton scattering length for $2E_0 = 500$ and 800 GeV and 1.35 scattering length for $2E_0 = 200$ GeV, so that $k^2 \approx 0.4$ and 0.55, respectively (k is the $e \to \gamma$ conversion coefficient). The laser wave length is 1.06 μm for all energies. The distance between conversion and interaction points is $b = \gamma\sigma_y$ for $2E_0 = 500$ and 800 GeV and $b = 2\gamma\sigma_y$

Table 3: Parameters of the photon collider at TESLA.

$2E_0$,GeV	200	500	800
λ_L [μm]/x	1.06/1.8	1.06/4.5	1.06/7.2
t_L/λ_{scat}	1.35	1	1
$N/10^{10}$	2	2	2
σ_z [mm]	0.3	0.3	0.3
$f_{rep} \times n_b$ [kHz]	14.1	14.1	14.1
$\gamma\epsilon_{x/y}/10^{-6}$ [m·rad]	2.5/0.03	2.5/0.03	2.5/0.03
$\beta_{x/y}$ [mm] at IP	1.5/0.3	1.5/0.3	1.5/0.3
$\sigma_{x/y}$ [nm]	140/6.8	88/4.3	69/3.4
b [mm]	2.6	2.1	2.7
$L_{e^-e^-}$(geom) [10^{34} cm^{-2}s^{-1}]	4.8	12	19
$L_{e^-e^-}(z > 0.65)$	0.03	0.07	0.095
$W_{\gamma\gamma,max}$ (GeV)	122	390	670
$L_{\gamma\gamma}(z > 0.8z_{m,\gamma\gamma})$ [10^{34}]	0.43	1.1	1.7
$W_{\gamma e,max}$ (GeV)	156	440	732
$L_{\gamma e}(z > 0.8z_{m,\gamma e})$ [10^{34}]	0.36	0.94	1.3
$L_{e^+e^-}$ [10^{34} cm^{-2}s^{-1}]	1.3	3.4	5.8

for $2E_0 = 200$ GeV. Simulation results presented below include nonlinear effects in the Compton scattering [36, 37]. Corresponding parameters $\xi^2 = 0.15, 0.2, 0.4$ for $2E_0 = 200, 500, 800$ GeV, respectively. From Table 3 one can see that for the same energy $L_{\gamma\gamma}(z > 0.8z_m) \approx (1/3)L_{e^+e^-}$.

Simultaneously with $\gamma\gamma$ collisions there are also γe collisions with somewhat lower luminosity, so one can study both types of collisions simultaneously. Residual electron-electron luminosity is very small due to the beam repulsion.

The normalized $\gamma\gamma$ luminosity spectra for $2E_0 = 500$ GeV and 800, 200 GeV are shown in Fig. 6. The luminosity spectra are decomposed in two parts: with the total helicity 0 and 2. Fig. 6 shows also luminosity spectra with additional cuts on the longitudinal momentum of the produced system, which suppress the low energy luminosity to a low level. In the case of only two jets one can restrict the longitudinal momentum using the acollinearity angle between jets ($H \to b\bar{b}, \tau\tau$, for example).

For the Higgs the production rate is proportional to $dL_0/dW_{\gamma\gamma}$ at $W_{\gamma\gamma} = M_H$. For the case considered, $M_H \approx 120\,\mathrm{GeV}$, and $x = 1.8$, $dL_0/dW_{\gamma\gamma} = 1.7 \times 10^{32}\,\mathrm{cm}^{-2}\mathrm{s}^{-1}/\,\mathrm{GeV}$. Note that the corresponding peak luminosity for NLC at the time of Snowmass2001 was 7 times smaller[10] and recent revised number is 2.8 times smaller [38]. In turn, TESLA also has large resources for

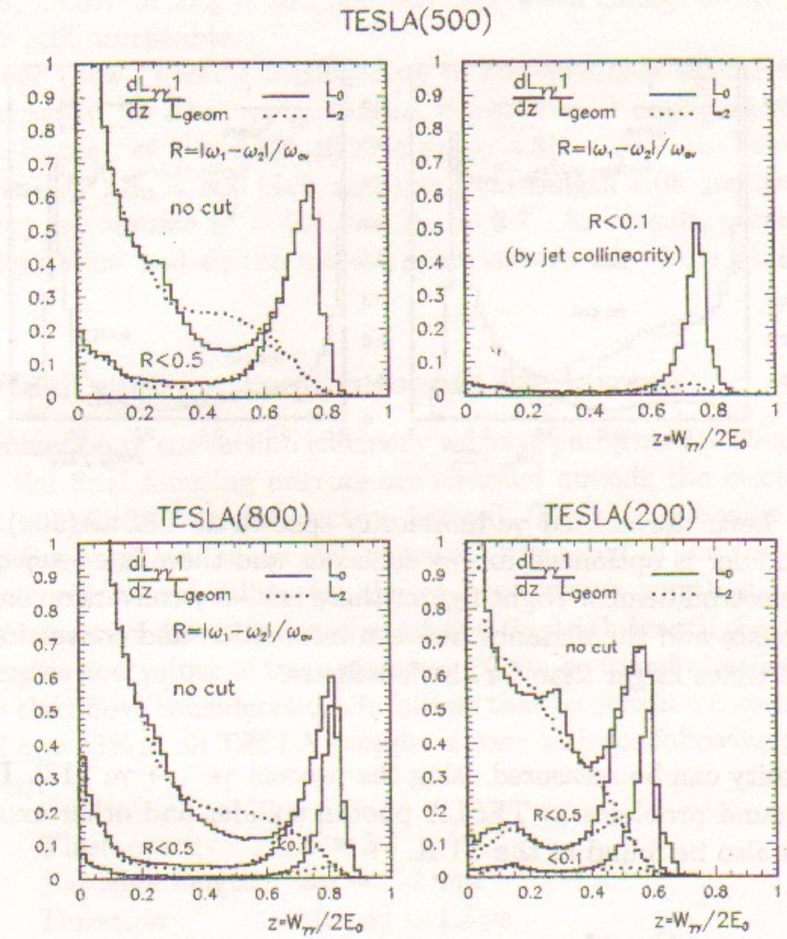

Figure 6: $\gamma\gamma$ luminosity spectra at TESLA. Solid line for total helicity of the two photons 0 and dotted line for total helicity 2. Dashed curves: luminosities with cuts on longitudinal momentum. See the text.

further improvement of the luminosity. It will be more clear after detailed optimization of the final focus (FF) system.

The normalized γe luminosity spectra for $2E_0 = 500$ GeV and parameters from Table 3 are shown in Fig. 7-left. For dedicated γe experiments one can convert only one electron beam, increase the distance between the conversion and the interaction points and obtain the γe luminosity spectrum with suppressed low energy part, Fig. 7-right.

The $\gamma\gamma$ luminosity distributions, including all their polarization characteristics, can be measured using processes $\gamma\gamma \to l^+l^-$ ($l = e, \mu$)[42, 13]. The

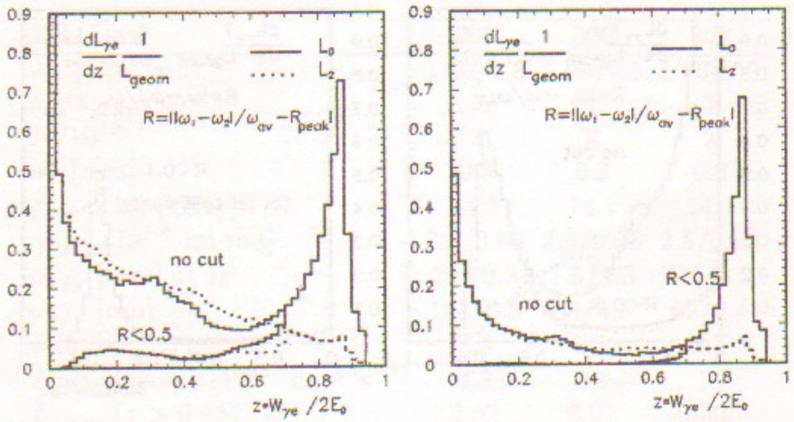

Figure 7: Left: normalized γe luminosity spectra at TESLA(500) when the photon collider is optimized for $\gamma\gamma$ collisions and there is $e \to \gamma$ conversion for both electron beams. Right figure: there is $e \to \gamma$ conversion only for one electron beam and the distance between interaction and conversion point is 1.05 cm, 5 times larger than for the left figure.

γe luminosity can be measured using the process $\gamma e^- \to \gamma e^-$[13]. Discussion of background problems at TESLA photon collider and other experimental issues can also be found in the TDR.

4 Lasers-Optics

A key element of photon colliders is a powerful laser system which is used for the $e \to \gamma$ conversion. The required parameters and possible schemes of lasers are discussed below.

4.1 Laser wavelength

There are two main parameters characterizing Compton scattering: x defined by Eq.1 and $\xi^2 = e^2\overline{B^2}\hbar^2/(m^2c^2\omega_0^2) = 2n_\gamma r_e^2\lambda/\alpha$ characterizing nonlinear effects in Compton scattering. At $\xi^2 \ll 1$ the electron scatters on one laser photon, at $\xi^2 \ll 1$ – on several. With grows of ξ^2 the spectrum becomes wider and is shifted to lower energies [37, 13], therefore it is preferable to have $\xi^2 << 1$. However, decrease of ξ^2 in the conversion leads inevitably to the increase of the required laser flash energy. For TESLA project we assume

$\xi^2 = 0.15, 0.3.0.4$ for $2E_0 = 200, 500, 800$ GeV when change of the luminosity spectra is still acceptable.

Another (now "good") consequence of the nonlinear effects is the shift of the threshold for e^+e^- pair creation in collision of laser and high energy photons. Instead of $x \approx 4.8[6, 8]$ it is $x_{th} = 4.8(1 + \xi^2)$. For the maximum TESLA energy $2E_0 = 800$ GeV and laser wavelength 1.06 μm $x \approx 7.2$. For this energy we assume $\xi^2 = 0.4$ and $x_{th} \approx 6.7$. As reasult, pair creation is practically absent and we can use the same laser in the whole TESLA energy region.

4.2 Flash energy, requirements for lasers

For optimization of conversion efficiency we have performed simulation asuming that the final focusing mirrors are situated outside the electron beams (without holes in mirrors for electron beams). The tilte of beams due to the crab crossing angle was taken into account. The result of the simulation [12] of the conversion probability for the electron bunch length $\sigma_z = 0.3$ mm, $\lambda = 1.06\,\mu$m, $x = 4.8$ as a function of the Rayleigh length Z_R for various flash energies and values of the parameter ξ^2 can be found elsewhere [12, 13].

From the above considerations it follows that to obtain a conversion probability of $k \approx 63\%$ at all TESLA energies a laser with the following parameters is required:

Flash energy	A ≈ 5 J
Rayleigh length	$Z_R \sim 0.4$ mm
Duration	$\tau(rms) \approx 1.5$ ps
Repetition rate	TESLA collision rate, $\nu \approx 14$ kHz
Average power	$P \approx 140$ kW (for one pass collision)
Wavelength	$\lambda \approx 1\,\mu$m (for all energies).

4.3 Laser schemes

All parameters for lasers are reasonable for exception of the repetition rate (average power). To overcome the "repetition rate" problem it is quite natural to consider a laser system where one laser bunch is used for the $e \to \gamma$ conversion many times. Two ways of multiple use of one laser pulse are considered for the Photon Collider at TESLA: an optical storage ring and an external optical cavity.

In the first scheme [12, 13], Fig.8, each laser bunch is used for the e$\to \gamma$ conversion about 12 times. The laser pulse is sent to the interaction region

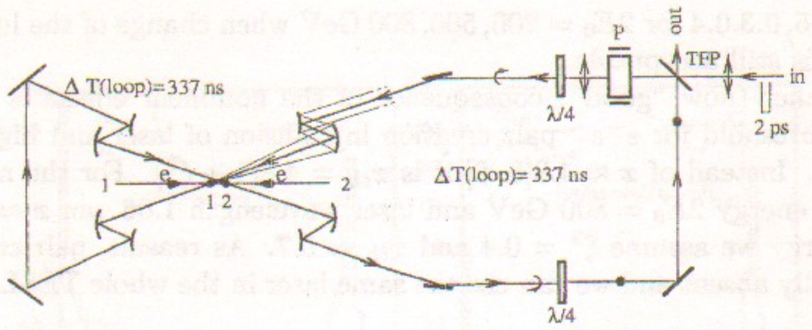

Figure 8: Optical trap (storage ring)

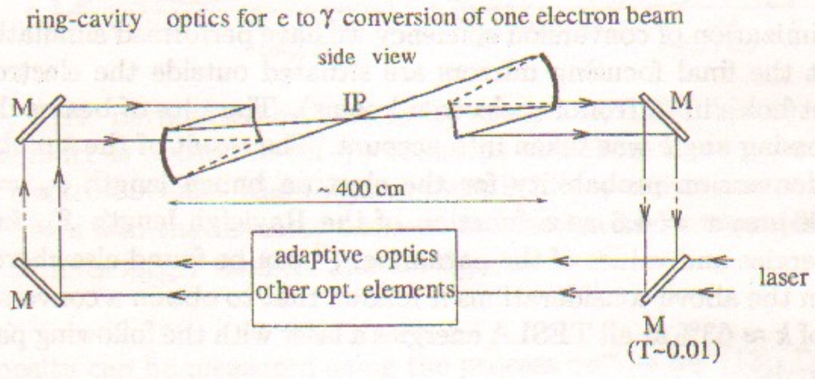

Figure 9: Ring type external optical cavity.)

where it is trapped in an optical storage ring. This can be done using Pockels cells (P), thin film polarizers (TFP) and 1/4-wavelength plates ($\lambda/4$). The maximum number of cycles is determined by reflection coefficients of mirrors and attenuation in the Pockels cell.

In the second scheme [18, 12, 43, 13], Fig.9, an "external" optical cavity is used. Using a train of low energy laser pulses one can create in the external cavity (with one mirror having small transmission) an optical pulse with an energy higher than in a laser pulse by a factor Q (cavity quality factor) and this pulse collides with electron bunches many times. As result the required laser power can be lower than in the one-pass case by factor of 50–100.

Development of laser technologies is being driven by several large programs, such as inertial fusion. This is a fortunate situation for photon colliders as we may benefit from the laser technology developments of the last 10–15 years which cost hundreds M$ per year. In the last decade the technique of short pulse powerful solid state lasers made an impressive step and

has reached petawatt (10^{15}) power levels and few femtosecond durations. Obtaining few joule pulses of picosecond duration is not a problem using modern laser techniques. The wave length of the most powerful lasers about 1 μm which is just optimum for the TESLA Photon Collider.

A free electron laser (FEL) is also attractive because it has a variable wave length and is based fully on the accelerator technology. The X-ray FEL with a wave length down to 1 nm is a part of the TESLA project. The same technology (only much easier) can be used for the construction of an FEL with 1 μm wave length for the Photon Collider [44]. However, at present we give preference to a solid laser, because it might be a large room–size system, while a FEL would be a large facility. For multi-TeV energies, where longer laser wave length will be required, a FEL may be the best choice.

The laser technologies most important for photon colliders are: chirped–pulse technique; diode pumping; laser materials with high thermo–conductivity; adaptive optics (deformable mirrors); disk amplifiers with gas (helium) cooling; large Pockels cells, polarizers; high power and high reflectivity multilayer dielectric mirrors; anti–reflection coatings. Now practically all components exist and we can just design the required system. Fortunately, this possibility has appeared almost exactly in the time when the physics community is ready for construction of linear colliders. Of course, design and construction of the laser system for the Photon Collider is not a simple task and needs many efforts. Development of the detailed scheme of a laser for the TESLA Photon Collider needs additional R&D in the next 2-3 years.

As the ECFA Panel in Europe and the Snowmass Study and the HEPAP panel in US have recommended the linear collider on the energy about 500 GeV as the next large HEP project (Asian physicists have also similar plans), it is very likely that in about one decade physicists will get a new very powerful instrument for study of matter: e^+e^-, $\gamma\gamma$, γe, e^-e^- collider.

The work has been partially supported by the INTAS 00-00679 grant.

References

[1] The NLC Design Group, *Zeroth-Order Design Report for the NLC*, LBNL-5424, SLAC-474, 1996, 2001 Report on the NLC sumbitted to Snowmass 2001, Fermilab-Conf 01-075, LBLL-47935, SLAC-R-571; Linear collider physics resource book for Snowmass 2001, By American Linear Collider Working Group, T. Abe et al., SLAC-R-570, May 2001.

[2] *Conceptual Design of a 500 GeV e^+e^- Linear Collider with Integrated X-Ray Laser Facility*, DESY 1997-048, ECFA 1997-182, DESY, 1997.

[3] *TESLA: The Superconducting electron positron linear collider with an integrated X-ray laser laboratory. Technical design report*, DESY 2001-011, ECFA 2001-209, TESLA Report 2001-23, DESY-TESLA-FEL-2001-05, March 2001.

[4] N. Akasaka et al., JLC Design Study, KEK-REPORT-97-1; ACFA Linear Collider Working group (K.Abe et al.) KEK-REPORT-2001-11, hep-ph/0109166.

[5] J.P. Delahaye et al., Acta Phys. Polon. **B30**:2029-2039 (1999); CERN-CLIC Note 463.

[6] I. F. Ginzburg, G. L. Kotkin, V. G. Serbo, and V. I. Telnov, *Pizma ZhETF*, 34:514, 1981 (*JETP Lett.* 34:491, 1982); *Nucl. Instrum. &Meth.*, **205**:47, 1983.

[7] I. F. Ginzburg, G. L. Kotkin, S. L. Panfil, V. G. Serbo, and V. I. Telnov. *Nucl. Inst. Meth.*, **A219**:5, 1984.

[8] V. I. Telnov, *Nucl. Instrum. &Meth.*, **A294**:72, 1990; **A355**:3, 1995.

[9] J. Gronberg, *Nucl. Instr. &Meth.* **A472**:61, 2001.

[10] Linear collider physics resource book for Snowmass 2001, By American Linear Collider Working Group, T. Abe et al., SLAC-R-570, May 2001, part 4, p.347, hep-ex/0106058.

[11] R. Brinkmann et al., *TESLA Conceptual Design, the Second Interaction Region for $\gamma\gamma$, γe collisions, Nucl. Instrum. &Meth.*, **A406**:13, 1998, hep-ex/9707017.

[12] V. Telnov, *Nucl. Instr. &Meth.* **A472**:43, 2001, hep-ex/0010033.

[13] B. Badelek et al., *TESLA Technical Design Report, Part VI, Ch.1. Photon collider at TESLA*, DESY 2001-011, ECFA 2001-209, TESLA Report 2001-23, hep-ex/0108012.

[14] I. Watanabe, et al, KEK-REPORT-97-17.

[15] T.Takahashi, *Nucl. Instr. &Meth.* **A472**:4, 2001.

[16] H. Burkhardt, *Nucl. Instr. &Meth.* **A472**:67, 2001.

[17] I. F. Ginzburg, *Proc. IX Intern. Workshop on Photon – Photon Collisions, San Diego, CA, USA*, p. 474, 1992, World Scientific.

[18] V. I. Telnov, Nucl. Phys. Proc. Suppl. **82**:359, 2000, hep-ex/9908005.

[19] V. Telnov, *Int. J. Mod. Phys.*, **A13**:2399, 1998, hep-ex/9802003.

[20] T. Barklow, In *Research Directions for the Decade. Proceedings, Summer Study on High-Energy Physics, Snowmass, USA*, p.440, 1990; J. F. Gunion and H. E. Haber, *Phys. Rev.*, **D48**:5109, 1993; D. L. Borden, D. A. Bauer, and D. O. Caldwell, *Phys. Rev.*, **D48**:4018, 1993.

[21] B. Grzadkowski and J. F. Gunion, *Phys. Lett.*, **B294**:361, 1992. hep-ph/9206262; J. F. Gunion and J. G. Kelly, *Phys. Lett.*, **B333**:110, 1994. hep-ph/9404343; M. Krämer, J. Kühn, M. L. Stong, and P. M. Zerwas, *Z. Phys.*, **C64**:21, 1994, hep-ph/9404280; K.Hagiwara, *Nucl. Instr. &Meth.* **A472**:12, 2001;

[22] S. Söldner-Rembold and G. Jikia, *Nucl. Instr. &Meth.* **A472**:133, 2001, hep-ex/0101056; (also M. Melles, ibid, **A472**:128, 2001 and [14]). hep-ph/0008125.

[23] D. A. Morris, T. N. Truong, and D. Zappala, *Phys. Lett.*, **B323**:421, 1994, hep-ph/9310244; I. F. Ginzburg and I. P. Ivanov, *Phys. Lett.*, **B408**:325, 1997, hep-ph/9704220; E. Boos, et al., *Phys. Lett.*, **B427**:189, 1998, hep-ph/9801359; E. Boos, et al., In *Proceedings of the Worldwide Study on Physics and Experiments with Future Linear e^+e^- Colliders*, vol. I, p. 498, Sitges, Spain, 1999.

[24] G. V. Jikia, *Phys. Lett.*, **B298**:224, 1993; G. Jikia, *Nucl. Phys.*, **B405**:24, 1993; M. S. Berger, *Phys. Rev.*, **D48**:5121, 1993; D. A. Dicus and C. Kao, *Phys. Rev.*, **D49**:1265, 1994.

[25] M. M. Mühlleitner, *Nucl. Instr. &Meth.* **A472**:139, 2001; M. M. Mühlleitner, M. Krämer, M. Spira, and P. M. Zerwas, Phys. Lett. **B508**:311, 2001, hep-ph/0101083.

[26] I. F. Ginzburg, M. Krawczyk, and P. Osland, *Nucl. Instr. &Meth.* **A472**:149, 2001.

[27] E. Asakawa, S. Y. Choi, K. Hagiwara, and J. S. Lee, *Phys. Rev.*, **D62**:115005, 2000, hep-ph/0005313.

[28] M. Klasen, *Nucl. Instr. &Meth.* **A472**:160, 2001, hep-ph/0008082; T. Mayer and H. Fraas, *Nucl. Instr. &Meth.* **A472**:165, 2001, hep-ph/0009048.

[29] F. Cuypers, G. J. van Oldenborgh, and R. Rückl, *Nucl. Phys.*, **B383**:45, 1992, hep-ph/9205209; *Nucl. Phys.*, **B409**:144, 1993, hep-ph/9302302; F. Cuypers, *Phys. Rev.*, **D49**:3075, 1994, hep-ph/9310327; A. Goto and T. Kon, *Europhys. Lett.*, **19**:575, 1992; T. Kon and A. Goto, *Phys. Lett.*, **B295**:324, 1992; C. Blöchinger, F. Franke, and H. Fraas. *Nucl. Instr. &Meth.* **A472**:144, 2001, hep-ph/0008167;

[30] D. S. Gorbunov, V. A. Ilyin, and V. I. Telnov, *Nucl. Instr. &Meth.* **A472**:171, 2001, hep-ph/0012175.

[31] N. Arkani-Hamed, S. Dimopoulos, and G. Dvali, *Phys. Lett.*, **B429**:263, 1998; *Phys. Rev.*, **D59**:086004, 1999; I. Antoniadis, N. Arkani-Hamed, S. Dimopoulos, and G. Dvali, *Phys. Lett.*, **B436**:257, 1998.

[32] T. G. Rizzo, *Nucl. Instr. &Meth.* **A472**:37, 2001; *Phys. Rev.*, **D60**:115010, 1999.

[33] E. Boos et al., *Nucl. Instr. &Meth.* **472**:100, 2001, hep-ph/0103090.

[34] *Proc. of Workshop on $\gamma\gamma$ Colliders*, Berkeley CA, USA, *Nucl. Instrum. &Meth.*, **A355**, 1995.

[35] *Proc. International Workshop On High-Energy Photon Colliders* (GG2000), Hamburg, Germany, 2000. *Nucl. Instr. &Meth.* **A472** (2001). http://www.desy.de/~gg2000/.

[36] I. F. Ginzburg, G. L. Kotkin, and S. I. Polityko, *Sov. J. Nucl. Phys.*, **37**:222, 1983; *Yad. Fiz.*, **40**:1495, 1984; *Phys. Atom. Nucl.*, **56**:1487, 1993.

[37] M. Galynskii et al., *Nucl. Instr. &Meth.* **A472**:276, 2001, hep-ph/0012338.

[38] D. Asner, J. Gronberg, J. Gunion, UCD-2001-8, hep-ph/0110320.

[39] W. Decking, *Nucl. Instr. &Meth.* **A472**:297, 2001.

[40] N. Walker, *Nucl. Instr. &Meth.* **A472**:291, 2001.

[41] P. Raimondi and A. Seryi, SLAC-PUB-8460, *Phys.Rev.Lett.* **86**:3779, 2001.

[42] V. I. Telnov, In *Workshop on Physics and Exper. with Linear e^+e^- Colliders, Waikoloa, USA*, p. 323, 1993, World Scientific.

[43] I. Will, T. Quast, H. Redlin, and W. Sandner, *Nucl. Instr. &Meth.* **A472**:79, 2001.

[44] E. L. Saldin, E. A. Schneidmiller, and M. V. Yurkov, *Nucl. Instr. &Meth.* **A472**:94, 2001.

V. Telnov

Photon Collider at Tesla

В.И. Тельнов

Фотонный коллайдер на TESLA

Ответственный за выпуск А.М. Кудрявцев
Работа поступила 14.11.2001 г.

Сдано в набор 23.11.2001 г.
Подписано в печать 23.11.2001 г.
Формат бумаги 60×90 1/8 Объем 1.7 печ.л., 1.4 уч.-изд.л.
Тираж 105 экз. Бесплатно. Заказ № 73

Обработано на IBM PC и отпечатано на
ротапринте "ИЯФ им. Г.И. Будкера" СО РАН,
Новосибирск, 630090, пр. академика Лаврентьева, 11.